Progress In Electromagnetics Research M, Vol. 80, 157–167, 2019

Direct Suspension Force Control of Hybrid Stator Bearingless Switched Reluctance Motor Based on Quasi-Continuous Three-Order Sliding Mode

Yonghong Huang*, Shanshan Shi, Ye Yuan, Yukun Sun, and Jie Xu

Abstract—In order to solve the problem of strong coupling between torque and suspension force of bearingless switching motor and the strong chattering of sliding mode control, a direct suspension force control method for hybrid stator bearingless switched reluctance motor based on quasi-continuous third-order sliding mode is proposed. According to the special structure of hybrid stator bearingless switched reluctance motor, the direct decoupling of torque and suspension force is realized. The suspension force control system adopts the direct suspension force control of the third-order sliding mode. By comparing with the second-order sliding mode control system under the condition of interference source and non-interference source, the results show that the designed control strategy has high precision, strong robustness, fast convergence speed, and it can effectively decrease vibration.

1. INTRODUCTION

Bearing switched reluctance motor (BSRM) combines the properties of magnetic bearing and switched reluctance motor (SRM) to realize the suspension of motor rotor, which has the advantages of high speed, high output power, low cost, and low loss [1–3]. These features make it have a good prospect in high speed flywheel energy storage and other applications.

Because of the coupling of suspension winding and torque winding, it is difficult to control the system, so the control system mainly adopts compound control [4–6]. In order to reduce the difficulty of control, the decoupling method of the suspension system and the torque system of the BSRM has become the research goal. Ref. [7] used the method of differential geometry to achieve radial suspension force decoupling. Ref. [8] adopts a neural network inverse model to decouple BSRM, and three closed-loop controllers are designed for pseudo-linear systems. Ref. [9] realizes the radial decoupling of a pseudo-linear system in SRM and parameter adjustment of the system according to dynamic features. Considering the change of parameters with time and the uncertainty of the system, a fuzzy compensator is designed to compensate the system in [10]. Ref. [11] proposes a new decoupling control strategy based on improved inverse system method, and a robust servo regulator is adopted for the decoupled plants. The above control strategies have their own different advantages, but these strategies will lead to the complexity of modeling. Therefore, for the BSRM with a complex structure, strong coupling, and nonlinearity, it is necessary to study a control method which can simultaneously consider system decoupling and simplify modeling.

When a BSRM system is subject to the disturbances from the parameter changes and external environment, the traditional sliding mode control can effectively solve the problem of large torque ripple and instability of the system because of its strong robustness and simple control algorithm [12, 13]. However, the nature of the low-order sliding mode control action is of the discontinuous type and

Received 28 January 2019, Accepted 2 April 2019, Scheduled 17 April 2019
* Corresponding author: Yonghong Huang (hyh@ujs.edu.cn).
The authors are with the School of Electrical and Information Engineering, Jiangsu University, Zhenjiang, Jiangsu 212013, China.

often accompanied by high-frequency chattering [14, 15], which presents the disadvantage that the high frequency exists in the system and will destroy the dynamic characteristics [16]. Therefore, the high-order sliding mode applied to the control system to solve the chattering [17, 18], which not only maintains the advantages of the traditional sliding mode, but also has higher precision and eliminates the limitation of relative degree, and the design of sliding surface is also flexible. Compared with the low-order sliding mode control which has the problems of discontinuous control and severe chattering, the chattering of the second-order sliding mode decreases in a certain extent, but the effects of these factors on the control system are also not negligible. Accordingly, further reducing the chattering of sliding mode control is a hot issue in sliding mode control.

In this paper, a 12/14 Hybrid Stator Bearingless Switched Reluctance Motor (HSBSRM) is taken as the research object, and the control system is divided into two parts: torque control system and suspension force control system. Common strategies for torque control are angle position control (APC), current chopping control (CCC), and voltage chopping control (VCC) [19]. Researchers have also proposed optimization methods [20–22] to reduce the pulsation of system. On this basis, in order to reduce the chattering and improve the robustness of the system, suspension force control subsystem is taken as a research focus, and the control system adopts direct suspension force control. The third-order sliding mode control based on the quasi-continuous high order sliding mode (HOSM) control algorithm [23–25] is applied to the control system to achieve stable control of the suspension force. Firstly, the principles of structure and suspension in the HSBSRM are introduced. The mathematical model of suspension force is analyzed, and the direct suspension force control method is proposed. Then the third-order sliding mode controller is designed by using quasi-continuous HOSM control algorithm. The simulation results show that the control system adopts direct suspension force control feasibility. Compared with the second-order sliding mode control, the direct suspension force control method with the third-order sliding mode can further eliminate chattering.

2. STRUCTURE AND OPERATING PRINCIPLE OF HSBSRM

The structure of 12/14 pole HSBSRM is shown in Fig. 1, and the motor torque coils need to be wound across stator teeth divided into phases A and phases B. The windings on poles A1, A2, A3, and A4 are connected in series to form A phase winding, and the windings on poles B1, B2, B3, and B4 are connected in series to form a B phase winding. T1, T2, T3, and T4 form the magnetic poles of the suspension force system. After the motor is energized, T3 and T4 poles generate x-axis direction suspension force, and T1 and T2 poles generate y-axis direction suspension force. By changing the current direction, the magnitude of air gap flux is changed, and the rotor is subjected to a suspension force in the positive or negative direction, so that the motor can be smoothly suspended.

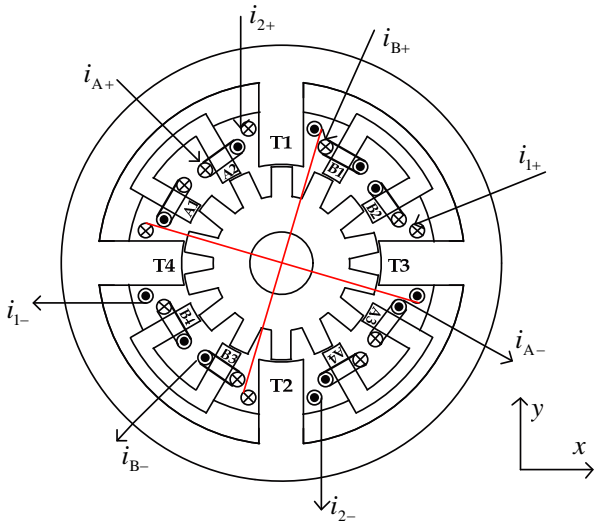

Figure 1. Structure of HSBSRM.

In order to simplify the analysis, assuming that the motor is in an ideal state without considering the hysteresis and eddy current loss, the voltage and flux equation of each phase are respectively given by:

$$U = Ri + \frac{d\Psi}{dt} \tag{1}$$

where Ψ is the flux, and i is the phase current of the conduction winding.

Due to the width of the pole arc of the suspension pole and the rotor pole pitch in the HSBSRM structure, the alignment area of the two poles remains unchanged, so the rotor position has little influence on the inductance of the suspension winding. The torque of the motor is proportional to the current and inductance, so the torque in the suspension winding is much smaller than the torque in the torque winding so that it can be ignored. Due to the above reasons, the coupling between the torque and the suspension force in the HSBSRM control strategy can be neglected to realize self-decoupling. This structure effectively solves the problem of strong coupling and reduces the complexity of the control system.

3. SUSPENSION FORCE CONTROL STRATEGY

3.1. Mathematical Model of Suspension Force

In the suspension system, the suspension force is divided into the suspension force F_x in x-axis direction and the suspension force F_y in y-axis direction, and suspension force F_x is analyzed by taking the x-axis direction as an example. When the system is in balance, the air gap length is l_0; the effective cross-sectional area of the magnetic circuit is A; the number of winding turns is n; the vacuum permeability is μ_0; the magnetic induction is B; and the current is i. The suspension force F can be obtained:

$$B = \mu_0 \frac{ni}{2l_0}, \tag{2}$$

$$F = \mu_0 n^2 A \frac{i^2}{2l_0}, \tag{3}$$

When the displacement of the rotor in the positive direction of the x-axis is x, the air gap between the positive direction of the x-axis and the rotor is $l - x$, and the air gap between the negative direction of the x-axis and the rotor is $l + x$. If the differential control method is adopted, considering the static bias current i_0, the current of the suspension winding in the positive direction of the x-axis is $i_0 - i_1$, and the current of the suspension winding in the negative direction of the x-axis is $i_0 + i_1$. Therefore, the suspension force F_1 in x-axis positive direction and suspension force F_2 in the x-axis negative direction are respectively:

$$\begin{aligned} F_1 &= \mu_0 n^2 A \frac{(i_0 - i_1)^2}{2(l_0 - x)^2} \\ F_2 &= \mu_0 n^2 A \frac{(i_0 + i_1)^2}{2(l_0 + x)^2}, \end{aligned} \tag{4}$$

The resultant force in the x-axis direction is:

$$F_x = F_1 - F_2, \tag{5}$$

Similarly, the mathematical model of the suspension force of HSBSRM in the y direction of the suspension system can also be obtained.

3.2. Direct Suspension Force Control

This paper has achieved double-loop control for the suspension control subsystem. The displacement constitutes the outer ring, and the inner ring is the suspension force ring. The direct suspension control can compensate the loss of the suspension force during the commutation in the traditional method, and the motor parameters have less influence on the control method, which reduces the difficulty of control modeling.

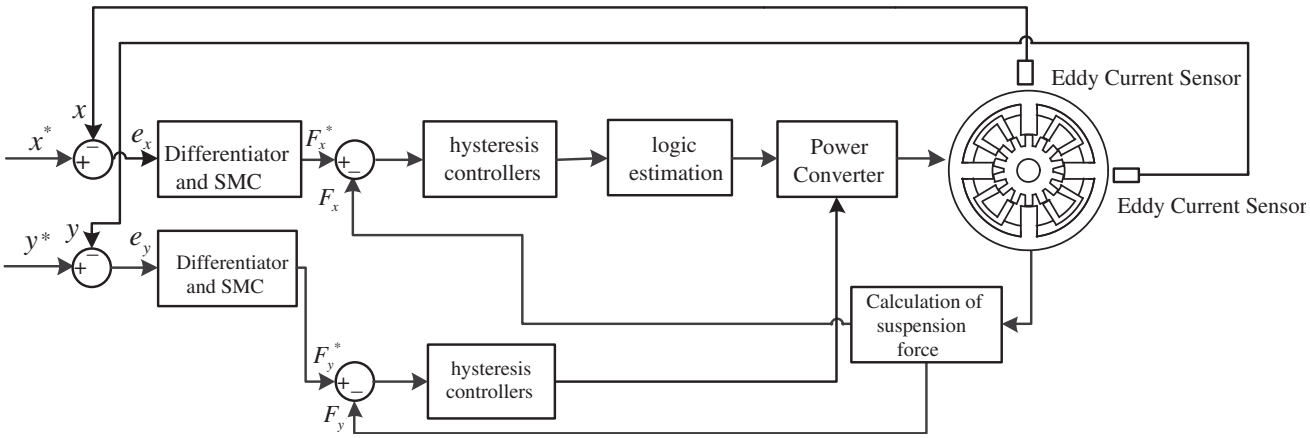

Figure 2. Suspension system control block diagram.

The suspension system control block diagram is shown in Fig. 2. Taking the x direction of the motor as an example, the suspension force F_x of the motor output is converted into displacement x by the force-displacement module, and the displacement x is compared with the reference of the displacement x^* to obtain the displacement error which acts as the input of the controller. Secondly, the reference suspension force $F_x{}^*$ which is output from the SMC is compared with the actual suspension force F_x to obtain e_{rx}. If $e_{rx} > 0$, the hysteresis loop controller can set the output signal 1; the main switch in the power converter is turned on; $F_x$increases in the positive direction of the x-axis gradually. If $e_{rx} < 0$, the hysteresis loop controller can set the output signal -1; the main switch in the power converter is turned off; F_x gradually increases in the negative direction of the x-axis. In this way, the suspension force F_x will be maintained within a certain range, accompanied by fluctuations, and finally it will complete the smooth operation of the motor suspension system and stabilize the displacement.

4. HIGH-ORDER SLIDING MODE CONTROLLER

The high-order sliding mode not only inherits the invariance of the traditional low-order sliding mode, but also has new features, which make the high-order sliding mode have the characteristics of high precision, fast response, and chattering suppression in the system.

In order to further eliminate the chattering in the control system and improve the control accuracy and response speed, the quasi-continuous HOSM algorithm is introduced into the sliding mode controller, and the second-order and third-order sliding mode control methods based on this algorithm are designed and compared.

4.1. The Design Method of Sliding Mode Controller

Since the sliding mode principle of the x-axis direction is the same as the the y-axis direction, the third-order sliding mode based on the quasi-continuous HOSM algorithm is described by taking the x-axis direction as an example. Establish a mathematical model of the controlled object:

$$\begin{aligned} e_x(t) &= x - x^* \\ \frac{dv_x}{dt} &= \frac{F_x}{m} \end{aligned} \tag{6}$$

where x is the radial displacement of the rotor in the x-axis direction, x^* the reference displacement of the rotor in the x-axis direction, v_x the rotational velocity of the rotor in the x-axis direction, F_x the suspension force in the x-axis direction, and m the quality of the rotor.

Design the sliding surface according to the sliding mode control theory:

$$S_x = \ddot{e}_x + \beta \dot{e}_x \tag{7}$$

where $\dot{e}_x$ is the first-order derivative of the displacement error, and $\ddot{e}_x$ is the second-order derivative of the displacement error.

The known suspension system equation is:

$$F_x = m\ddot{x} \tag{8}$$

where $\ddot{x}$ is the second derivative of the displacement in the x-axis direction, $\ddot{y}$ the second derivative of the displacement in the y-axis direction, and F_x ithe suspension force in the x-axis direction. Assuming that $F_x = u_1$, $\dot{F}_x = u_2$, it can be concluded separately that the relative orders of the system are $r = 2$ and $r = 3$, therefore, the control rates of second-order and third-order sliding mode controllers are designed according to the quasi-continuous algorithm:

When $r = 2$:

$$\begin{cases} \varphi_1 = \dot{S}_x + |S_x|^{\frac{1}{2}} \operatorname{sign}(S_x) \\ N_1 = |S_x|^{\frac{1}{2}} + |S_x| \\ u_1 = -\alpha_1 \dfrac{\varphi_1}{N_1} \end{cases} \tag{9}$$

When $r = 3$:

$$\begin{cases} \varphi_2 = \ddot{S}_x + 2\left(\left|\dot{S}_x\right| + |S_x|^{\frac{2}{3}}\right)^{-\frac{1}{2}} \left[\dot{S}_x + |S_x|^{\frac{2}{3}} \operatorname{sign}(S_x)\right] \\ N_2 = \left|\ddot{S}_x\right| + 2\left(\left|\dot{S}_x\right| + |S_x|^{\frac{2}{3}}\right)^{\frac{1}{2}} \\ u_2 = -\alpha_2 \dfrac{\varphi_2}{N_2} \end{cases} \tag{10}$$

where $\operatorname{sign}(S_x)$ is a symbol function; u_1 and u_2 are the control rates of the second-order and third-order sliding mode controllers in the x-axis direction respectively; and α_1, α_2 are adjustable parameters. If α_x is sufficiently large within a certain time, then S_x, $\dot{S}_x$, $\ddot{S}_x \to 0$. $\dot{S}_x$ is the first-order differential term of the sliding amount S_x, and $\ddot{S}_x$ is the second-order differential term of the sliding amount S_x. u_1 and u_2 are continuous except for $S_x = \dot{S}_x = \ddot{S}_x = 0$, so that the actual control can be obtained:

$$\begin{cases} r = 2, \quad F_x = \displaystyle\int u_1 dt \\ r = 3, \quad F_x = \displaystyle\int u_2 dt \end{cases} \tag{11}$$

4.2. A Design Method for Differential Controller

In fact, the above values cannot be obtained by the feedback of the sliding mode control system. In order to obtain the derivative of slip values, a differential controller designed by Levent is introduced to estimate these values [26]. In the switched reluctance motor output feedback controller, S_x, $\dot{S}_x$, and $\ddot{S}_x$ are replaced by z_{x0}, z_{x1}, and z_{x2}:

$$\begin{cases} \dot{z}_{x0} = v_{x0} \\ v_{x0} = -\lambda_0 L^{\frac{1}{3}} |z_{x0} - S_1|^{\frac{2}{3}} \operatorname{sign}(z_{x0} - S_1) + z_{x1} \\ \dot{z}_{x1} = v_{x1} \\ v_{x1} = -\lambda_1 L^{\frac{1}{2}} |z_{x1} - v_{x0}|^{\frac{1}{2}} \operatorname{sign}(z_{x1} - v_{x0}) + z_{x2} \\ \dot{z}_{x2} = -\lambda_2 L \operatorname{sign}(z_{x2} - v_{x1}) \end{cases} \tag{12}$$

where v_{x0}, v_{x1}, and v_{x2} are the values of the x-axis direction, which are set by the differentiator, then these values obtained by the differentiator are substituted into the third-order sliding mode displacement controller, and finally following formula will be obtained:

When $r = 2$:

$$\begin{cases} \varphi_{11} = z_{x1} + |z_{x0}|^{\frac{1}{2}} \operatorname{sign}(z_{x0}) = \varphi_1 \\ N_{11} = |z_{x0}|^{\frac{1}{2}} + |z_{x0}| = N_1 \\ u_{11} = -\alpha_1 \dfrac{\varphi_{11}}{N_{11}} \end{cases} \tag{13}$$

When $r = 3$:

$$\begin{cases} \varphi_{21} = z_{y2} + 2\left(|z_{y1}| + |z_{y0}|^{\frac{2}{3}}\right)^{-\frac{1}{2}} \cdot \left[z_{y1} + |z_{y0}|^{\frac{2}{3}} \operatorname{sign}(z_{y0})\right] = \varphi_2 \\ N_{21} = |z_{y2}| + 2\left(|z_{y1}| + |z_{y0}|^{\frac{2}{3}}\right)^{\frac{1}{2}} = N_2 \\ u_{21} = -\alpha_2 \dfrac{\varphi_{21}}{N_{21}} \end{cases} \tag{14}$$

Therefore, the design of the sliding mode displacement controller is:

$$\begin{cases} r = 2, \quad F_x = \int u_{11} dt \\ r = 3, \quad F_x = \int u_{21} dt \end{cases} \tag{15}$$

The Lyapunov second method is used to prove the existence of the sliding mode in the suspension system, and it meets the requirements of accessibility and stability. Therefore, prove the stability of the error dynamic system in Eq. (8): select the Lyapunov function as:

$$V = \frac{1}{2} S_x^2 \tag{16}$$

Let $x_1 = x$, $x_2 = \dot{x}_1$, so according to Equation (8), the equation of state is

$$\begin{cases} \dot{x}_1 = \dot{x} \\ \dot{x}_2 = \dfrac{1}{m} F_x = \dfrac{1}{m} \int u_2 \\ y = x_1 \end{cases} \tag{17}$$

Deriving Equations (6) and (7) respectively:

$$\begin{cases} \dot{e} = x_2 \\ \ddot{e} = \dot{x}_2 = \dfrac{1}{m} \int u_2 \\ e = \ddot{x}_2 = \dfrac{1}{m} u_2 \end{cases} \tag{18}$$

$$\dot{S}_x = e + \beta \ddot{e} = \frac{1}{m} u + \beta \dot{x}_2$$

where $\beta > 0$, deriving Equation (16) and substituting Equations (17), (18) to it

$$\dot{V} = S_x \dot{S}_x = S_x \left(\frac{1}{m} u + \beta \dot{x}_2\right) \tag{19}$$

Combining Equation (17), since the suspension force F_x is bounded, so that $\beta \dot{x}_2$ must be bounded, let $\beta \dot{x}_2 \leq M$, the following formula can be obtained:

$$\begin{aligned} &\left(\left|\dot{S}_x\right| + |S_x|^{\frac{2}{3}}\right)^{-\frac{1}{2}} \left[\dot{S}_x + |S_x|^{\frac{2}{3}} \operatorname{sign}(S_x)\right] \leq \left(\left|\dot{S}_x\right| + |S_x|^{\frac{2}{3}}\right)^{\frac{1}{2}} \\ &\dot{V} \leq M \|S_x\| + S_x \left(-\alpha_2 \frac{\ddot{S}_x + 2\left(\left|\dot{S}_x\right| + |S_x|^{\frac{2}{3}}\right)^{\frac{1}{2}}}{\ddot{S}_x + 2\left(\left|\dot{S}_x\right| + |S_x|^{\frac{2}{3}}\right)^{-\frac{1}{2}}}\right) \\ &\dot{V} \leq M \|S_x\| - \alpha_2 \|S_x\| \end{aligned} \tag{20}$$

It can be known from Equation (20) that only parameter α_2 is greater than the upper bound M of the suspension force F_x, and the stability of the control system can be ensured through the Lemma's theorem.

5. SIMULATION RESULTS AND DISCUSSIONS

In order to verify the effectiveness of the direct torque control based on the quasi-continuous third-order sliding mode of HSBSRM, the HSBSRM suspension force subsystem control model is established based on the Simulink simulation platform. Parameters of the simulation model are shown in Table 1.

Table 1. Simulation parameters.

Parameters	Value
hysteresis width of suspension force/mm	0.1
Resistance/Ω	1
self-inductance/H	0.013
mass of rotor/kg	5
simulation time/s	1.2

In order to verify the robustness, the non-interference condition and interference condition are set to simulate the suspension force control strategy, respectively. Simultaneously, in order to verify the effectiveness of suppressing the chattering, the second-order sliding mode controller and third-order sliding mode controller are respectively applied to the control strategy for comparison.

5.1. Simulation Results and Analysis under Non-Interference Signals

The simulation model of the suspension force control under the condition of non-interference signal is established. The rotor displacement of HSBSRM is shown in Fig. 3, and the suspension ripple of HSBSRM is shown in Fig. 4. The dynamic response of the displacement based on the second-order sliding mode controller is shown in Fig. 3(a). The displacement can be quickly and stably balanced after 0.1 s, and it shows that the system has good dynamic characteristics, but it has severe chattering, and the displacement fluctuation ranges from 7×10^{-6} to 9×10^{-6} m. Fig. 3(b) shows dynamic response of the displacement based on the quasi-continuous third-order sliding mode controller. The displacement also maintains a steady state after 0.1 s, and the displacement fluctuation is around 7×10^{-6} m. Obviously, this chattering is smaller than Fig. 3(a). It is clear that the waveform is smoother, and there is almost no chattering of the displacement after 0.2 s.

The dynamic response of the suspension force ripple based on the second-order sliding mode controller is shown in Fig. 4(a). The range of the suspension force is from −5 to 5N, and the response curve has high frequency jitter obviously. Fig. 4(b) is the dynamic response of the suspension force based on the Quasi-continuous third-order sliding mode controller. The suspension force ranges from −3 to 4N, and the waveform is smoother than that in Fig. 4(a). It is clear that the suspension force pulsation is reduced by 30% and that the system response has a slight jitter before 0.4 s, and then it tends to be smooth.

5.2. Results and Analysis under Interference Signals

In order to analyze the robustness of the control system, an interference signal is introduced to the radial direction in the simulation model at 0.6 s. The displacement of the HSBSRM rotor is shown in Fig. 5, and the suspension force pulsation is shown in Fig. 6. Fig. 5(a) shows the displacement of the second-order sliding mode control under interference. The rotor position returns to the original position about 0.15 s after the disturbance. Fig. 5(b) shows the displacement based on the quasi-continuous third-order sliding mode controller under interference. The rotor position appears shaken after being disturbed, but it can quickly return to a stable state within 0.05 s, which is 66% faster than the speed of Fig. 5(a).

The dynamic response of the suspension force ripple based on the second-order sliding mode controller under interference is shown in Fig. 6(a). After being disturbed, the system suspension force

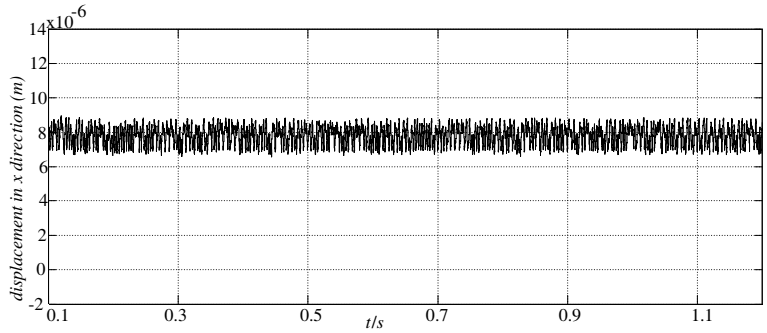

(a) the displacement based on the second-order sliding mode controller

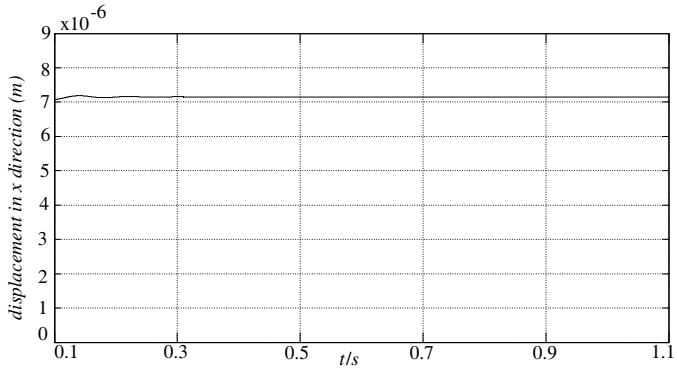

(b) the displacement based on the third-order sliding mode controller

Figure 3. Rotor displacement of HSBSRM with Non-interference signals.

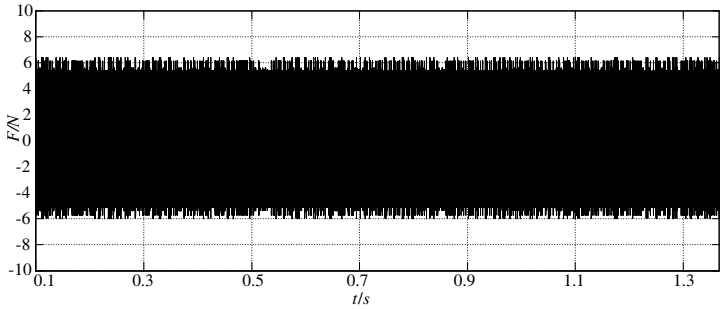

(a) the suspension force ripple based on the second-order sliding mode controller

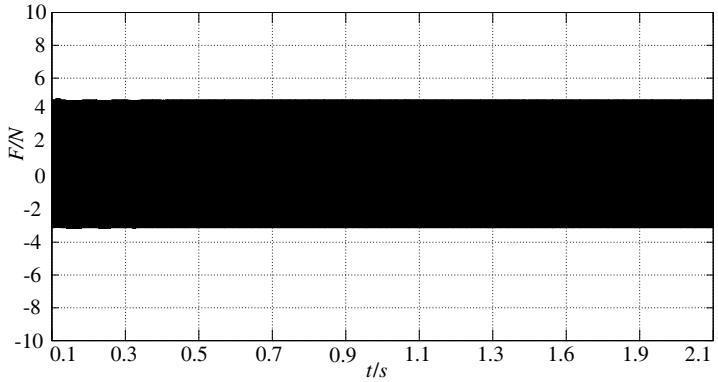

(b) the suspension force ripple based on the third-order sliding mode controller

Figure 4. Suspension force ripple of HSBSRM with Non-interference signals.

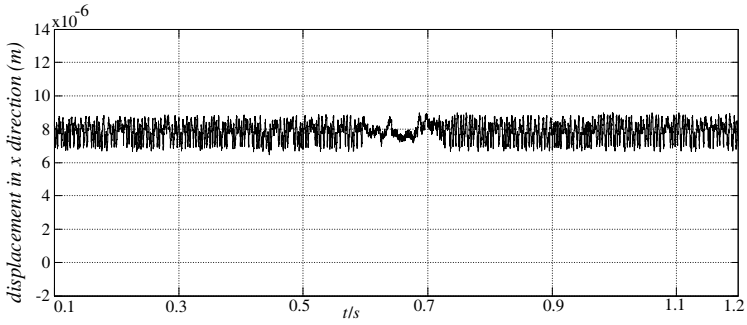

(a) the displacement of the second-order sliding mode control

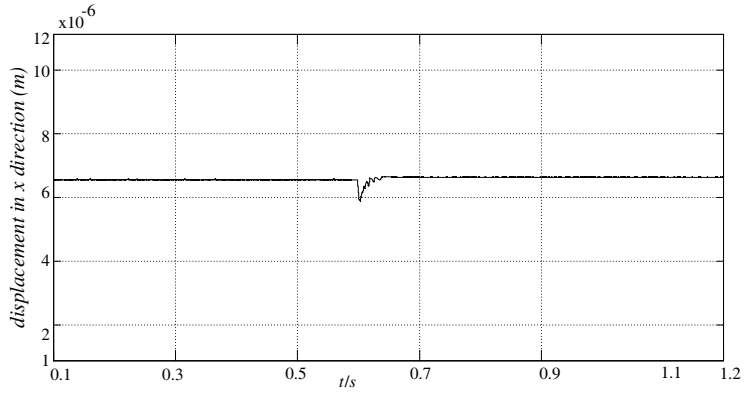

(b) the displacement based on the third-order sliding mode controller

Figure 5. Rotor displacement of HSBSRM with interference signals.

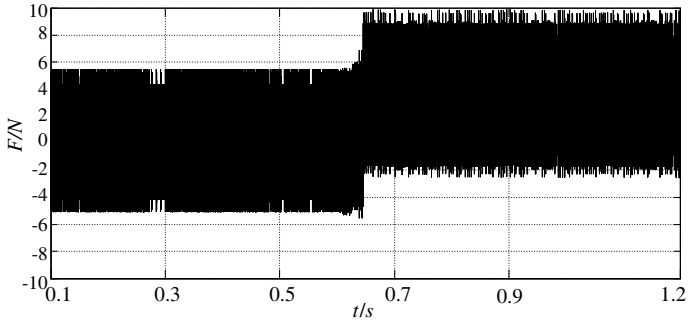

(a) the suspension force ripple based on the second-order sliding mode controller

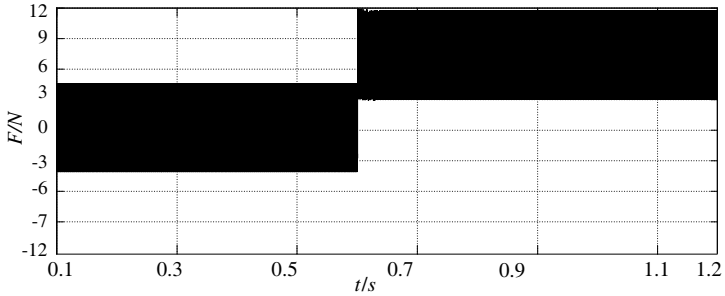

(b) the suspension force ripple based on the third-order sliding mode controller

Figure 6. Suspension force ripple of HSBSRM with interference signals.

has obvious large jitter. Fig. 6(b) is the dynamic response of the suspension force ripple based on the quasi-continuous third-order sliding mode controller under interference. The system suspension force ripple is smaller than that in Fig. 6(a), and the waveform is smoother.

It can be seen that the quasi-continuous third-order sliding mode controller system has the features of higher accuracy, robustness, and fast response. It has obvious effects on the suppression of chattering. This method reduces the jitter of the displacement and the suspension force during the control process, and improves the displacement recovery speed. It can also improve recovery speed of the displacement and the anti-jamming capability of the suspension under interference.

6. CONCLUSION

In this paper, a direct suspension force control strategy under the third-order sliding mode based on quasi-continuous algorithm is proposed for the HSBSRM to maintain the stability of suspension system. The direct torque control idea is introduced into the suspension force control method. Due to the discontinuity of the traditional sliding mode control, the buffeting of the suspension system will be caused which will affect the accuracy and stability of the control system, so the third-order sliding mode controller in the quasi-continuous algorithm is combined with the direct suspension force control method. The simulation results show that the direct suspension force control strategy avoids the modeling difficulties and simplifies the complexity of modeling. The third-order sliding mode in the control system has better suppression of the suspension force ripple than the second-order sliding mode control, with higher precision and strong robustness, which further effectively reduces the chattering of the system and the effect of vibration on system stability.

REFERENCES

1. Wang, H., J. Liu, J. Bao, et al., "A novel bearingless switched reluctance motor with a biased permanent magnet," *IEEE Transactions on Industrial Electronics*, Vol. 61, No. 12, 6947–6955, 2014.
2. Choudhury, M. D., F. Ahmed, G. Kumar, et al., "Design methodology for a special single winding based bearingless switched reluctance motor," *The Journal of Engineering*, Vol. 2017, No. 7, 274–284, 2017.
3. Wang, H., S. Tang, and B. Xue, "New type 12/14 bearingless switched reluctance motor with double windings," *IET Electric Power Applications*, Vol. 9, No. 7, 478–485, 2015.
4. Xin, C., S. Qin, C. Liu, et al., "Direct control of torque and levitation force for dual-winding bearingless switched reluctance motor," *Electric Power Systems Research*, Vol. 145, 214–222, 2017.
5. Chen, L. and W. Hofmann, "Speed regulation technique of one bearingless 8/6 switched reluctance motor with simpler single winding structure," *IEEE Transactions on Industrial Electronics*, Vol. 59, No. 6, 2592–2600, 2012.
6. Cao, X., Q. Sun, C. Liu, et al., "Direct control of torque and levitation force for dual-winding bearingless switched reluctance motor," *Electric Power Systems Research*, Vol. 145, 214–222, 2017.
7. Takemoto, M., A. Chiba, H. Akagi, et al., "Torque and suspension force in a bearingless switched reluctance motor," *Electrical Engineering in Japan*, Vol. 157, No. 2, 72–82, 2010.
8. Xun, Y. K., Y. H. Zhou, and X. F. Ji, "Decoupling control of bearingless switched reluctance motor with neural network inverse system method," *Proceedings of the Csee*, Vol. 31, No. 30, 117–123, 2011.
9. Wang, X.-L. and B.-M. Ge, "Radial suspending inverse-system method control for magnetic suspending switched reluctance motor," *Electric Machines and Control*, Vol. 13, No. 03, 356–360, 2009.
10. Cao, X., Z. Deng, G. Yang, and X. Wang, "Independent control of average torque and radial force in bearingless switched-reluctance motors with hybrid excitations," *IEEE Trans. Power Electron.*, Vol. 24, No. 5, 1376–1385, Jul. 2009.

11. Zhu, Z. Y., Y. K. Sun, and Y. Yuan, "Decoupling control for dual-winding bearingless switched reluctance motor based on improved inverse system method," *Mathematical Problems in Engineering*,, 1–17 2017.
12. Zhao, Y., S. H. Wu, H. H. Liu, et al., "Sliding mode control of switched reluctance motor with high torque in low speed," *Advanced Materials Research*, 694–697, 2085–2088, 2013.
13. Rafael, S., P. J. C. Branco, and A. J. Pires, "Sliding mode angular position control for an 8/6 switched reluctance machine: Theoretical concept, design and experimental results," *Electric Power Systems Research*, Vol. 129, 62–74, 2015.
14. Feng, Y., F. Han, and X. Yu, "Chattering free full-order sliding-mode control," *Automatica*, Vol. 50, No. 4, 1310–1314, 2014.
15. Ramos, R., D. Biel, E. Fossas, et al., "Sliding mode controlled multiphase buck converter with interleaving and current equalization," *Control Engineering Practice*, Vol. 21, No. 5, 737–746, 2013.
16. Rafiq, M., S. U. Rehman, F. U. Rehman, et al., "A second order sliding mode control design of a switched reluctance motor using super twisting algorithm," *Simulation Modelling Practice & Theory*, Vol. 25, No. 6, 106–117, 2012.
17. Li, L., L. Sun, and S. Zhang, "Mean deviation coupling synchronous control for multiple motors via second-order adaptive sliding mode control," *Isa Transactions*, Vol. 62, 222–235, 2016.
18. Hamida, M. A., J. D. Leon, and A. Glumineau, "High-order sliding mode observers and integral backstepping sensorless control of IPMS motor," *International Journal of Control*, Vol. 87, No. 10, 2176–2193, 2014.
19. Hao, C., H. Yang, Y. Chen, et al., "Reliability assessment of the switched reluctance motor drive under single switch chopping strategy," *IEEE Transactions on Power Electronics*, Vol. 31, No. 3, 2395–2408, 2016.
20. Krasovskii, A. B., "Studies of torque ripple in a switched reluctance motor under a controlled average torque value in a low-velocity mode," *Russian Electrical Engineering*, Vol. 88, No. 5, 247–252, 2017.
21. Jin, Y., B. Bilgin, and A. Emadi, "An extended-speed low-ripple torque control of switched reluctance motor drives," *IEEE Transactions on Power Electronics*, Vol. 30, No. 3, 1457–1470, 2015.
22. Shao, J., Z. Deng, and Y. Gu, "Fault-tolerant control of position signals for switched reluctance motor drives," *IEEE Transactions on Industry Applications*, Vol. 53, No. 3, 2959–2966, 2017.
23. Levant, A., "Quasi-continuous high-order sliding-mode controllers," *IEEE Transactions on Automatic Control*, Vol. 50, No. 11, 1812–1816, 2012.
24. Pukdeboon, C., A. S. I. Zinober, and M. W. L. Thein, "Quasi-continuous higher order sliding-mode controllers for spacecraft-attitude-tracking maneuvers," *IEEE Transactions on Industrial Electronics*, Vol. 57, No. 4, 1436–1444, 2010.
25. Ma, L., Y. Zhang, X. Yang, et al., "Quasi-continuous second-order sliding mode control of buck converter," *IEEE Access*, Vol. 6, 17859–17867, 2018.
26. Levant, A., "Higher-order sliding modes, differentiation and output-feedback control," *International Journal of Control*, Vol. 76, No. 9–10, 924–941, 2003.